Zero-bias conductance in carbon nanotube quantum dots

Frithjof B. Anders,[1] David E. Logan,[2] Martin R. Galpin,[2] and Gleb Finkelstein[3]

[1]*Institut für Theoretische Physik, Universität Bremen, P.O. Box 330 440, D-28334 Bremen, Germany*
[2]*Physical and Theoretical Chemistry, Oxford University, South Parks Road, Oxford OX1 3QZ, UK*
[3]*Department of Physics, Duke University, Durham, North Carolina 27708, USA*
(Dated: January 21, 2008)

We present numerical renormalization group calculations for the zero-bias conductance of quantum dots made from semiconducting carbon nanotubes. These explain and reproduce the thermal evolution of the conductance for different groups of orbitals, as the dot-lead tunnel coupling is varied and the system evolves from correlated Kondo behavior to more weakly correlated regimes. For integer fillings $N = 1, 2, 3$ of an $SU(4)$ model, we find universal scaling behavior of the conductance that is distinct from the standard $SU(2)$ universal conductance, and concurs quantitatively with experiment. Our results also agree qualitatively with experimental differential conductance maps.

Introduction: Carbon nanotubes have generated immense interest due to their rich transport properties [1]. Their small capacitance generates a Coulomb blockade regime at low temperatures [2], and a single electron transistor [2, 3] can be made out of weakly coupled nanotubes. The Kondo effect, studied in transition metal ions and rare earth compounds for some fifty years [4, 5], is now equally a classic hallmark of many-body physics in nanoscale devices, including carbon nanotubes [6] as well as semiconducting quantum dots, molecules and magnetic adatoms on metallic surfaces (for a review see [7]).

While the 'standard' Kondo effect arising in nanodevices is the orbitally non-degenerate, spin-$\frac{1}{2}$ ($SU(2)$) Kondo effect [4], it is known that in quantum dots made from high quality nanotubes, a series of *two* spin-degenerate orbitals originates from the two electronic sub-bands [8, 9]. Consecutive filling of these orbitals should thus yield an $SU(4)$-type Kondo effect [4, 10, 11, 12, 13, 14, 15, 16, 17, 18, 19, 20]. This has indeed been observed in recent experiments [10, 11, 12], including in particular systematic exploration of the $SU(4)$ conductance regimes [12] via careful control of sample contact transparency.

In this paper, we present a consistent picture which explains the experimental zero bias conductance [12]. We study the thermal evolution of the conductance as a function of applied gate voltage, for an $SU(4)$ Anderson model, using Wilson's numerical renormalization group (NRG) [5, 21] (previous NRG work [14, 15, 16, 17, 18, 19] has been confined to $T = 0$); and show that on progressive increase of the dot-lead tunnel couplings, the system exhibits a rich evolution from correlated Kondo behavior with strong associated Coulomb blockade peaks in the zero-bias conductance, through to a weaker coupling regime where charge fluctuations are significant and Coulomb blockade oscillations suppressed. We obtain universal scaling functions for the zero-bias conductance, which deviate significantly from standard $SU(2)$ Kondo scaling (reflecting the different universality class of our model); and show that this captures experiment quantitatively.

Theory: Interacting quantum dots, molecular junctions and other nano-devices are modelled by the interacting region $\mathcal{H}_{imp}$, a set of non-interacting reservoirs $\mathcal{H}_B$ and a coupling between the subsystems $\mathcal{H}_T$: $\mathcal{H} = \mathcal{H}_{imp} + \mathcal{H}_B + \mathcal{H}_T$. For the carbon nanotube quantum dot we restrict ourselves to the filling of one shell comprising two degenerate orbitals, and consider the local Hamiltonian $\mathcal{H}_{imp} = \frac{1}{2}U(\hat{N} - N_g)^2$. Here $\hat{N} = \sum_{\alpha\sigma} d^\dagger_{\alpha\sigma} d_{\alpha\sigma} = \sum_{\alpha\sigma} \hat{n}_{\alpha\sigma}$, where $d^\dagger_{\sigma\alpha}$ creates a σ-spin electron in orbital $\alpha = 1, 2$, the charging energy $U = e^2/C \equiv E_C$ with dot capacitance C, and N_g denotes the dimensionless external gate voltage. Equivalently,

$$\mathcal{H}_{imp} = E_d \hat{N} + \frac{1}{2}U \sum_{m,m'(m'\neq m)} \hat{n}_m \hat{n}_{m'} \qquad (1)$$

with level energy $E_d = \frac{U}{2}(1 - 2N_g)$ and $m \equiv (\alpha, \sigma)$ a flavor index. For the isolated dot, with integer ground state charge ($\langle \hat{N} \rangle =$) $N_d = 0 - 4$, the edges in the Coulomb blockade staircase between charge N_d and N_d+1 occur for half-integral $N_g = \frac{1}{2}(2N_d+1)$ (ie $E_d = -UN_d$). In Eq.(1) we have taken $U' = U$, with U [U'] the intra- [inter-] orbital Coulomb repulsion, and have also neglected an exchange splitting, J. This is consistent with the argument [22] that for carbon nanotubes, $U' \simeq U$ and J is much smaller than the charge fluctuation scale; and is known to be compatible with the nanotube data [23].

The tunneling to the two leads $\nu = L, R$ is assumed to be spin and orbital conserving [12, 18],

$$\mathcal{H}_T = \sum_{\alpha,\nu} \tilde{t}_\nu \sum_{k,\sigma} \left(c^\dagger_{k\sigma\alpha\nu} d_{\sigma\alpha} + d^\dagger_{\sigma\alpha} c_{k\sigma\alpha\nu} \right) \qquad (2)$$

such that the overall $\mathcal{H}$ has $SU(4)$ symmetry. Only the binding combination of lead states, $c_{k\sigma\alpha} = \frac{1}{t} \sum_\nu \tilde{t}_\nu c_{k\sigma\alpha\nu}$ with $t = [\tilde{t}_L^2 + \tilde{t}_R^2]^{\frac{1}{2}}$, then couples to the dot. We can thus drop the lead index ν and consider one effective lead:

$$\mathcal{H}_B = \sum_{k\sigma\alpha} \epsilon_k c^\dagger_{k\sigma\alpha} c_{k\sigma\alpha} . \qquad (3)$$

Note however that the different couplings still enter via the conductance prefactor $G_0 = (e^2/h)4\Gamma_L\Gamma_R/(\Gamma_L +$

$\Gamma_R)^2$, which reaches the unitary limit of e^2/h for a perfect symmetric channel $\Gamma_L = \Gamma_R$ [24], where $\Gamma_\nu = \pi \tilde{t}_\nu^2 \rho$ with ρ the density of states of the leads at the Fermi energy.

Method: We solve the Hamiltonian accurately using the powerful NRG approach [5]; for a recent review see [21]. Finite temperature NRG Green's functions are calculated using the recently developed algorithm [25], employing a complete basis set of the Wilson chain. Originally derived for real-time dynamics of quantum impurities out of equilibrium [26], this ensures that the spectral sum-rule is exactly fulfilled and the NRG occupancy accurately reproduced. The self-energy of the Green function is calculated in the usual way [21].

The local Green function determining transport is given by $G_\alpha^d(z) = [z - \epsilon - \Delta(z) - \Sigma(z)]^{-1}$ with $z = \omega + i0^-$, $\Delta = \sum_\nu \tilde{t}_\nu^2 \sum_k [z - \epsilon_k]^{-1}$ the dot-lead hybridization, and $\Sigma(z)$ the interaction self-energy; the local spectrum is $D(\omega, T) = \frac{1}{\pi} \Im m G_\alpha^d(z)$. At $T = 0$, the Friedel sum rule [27, 28] relates the number of impurity electrons N_{imp} to the conduction electron scattering phase shift $\delta = \pi N_{imp}/N$, where N is the number of channels (here $N = 4$). $N_{imp} = N_d + \Delta N$ includes all electrons on the quantum dot ($N_d = \langle \sum_{\alpha,\sigma} \hat{n}_{\alpha\sigma} \rangle$) *and* the number of displaced electrons in the bath ΔN [28], and can be obtained directly from the NRG [5]. For a vanishing $\Im m \Sigma_{\sigma\alpha}(i0^-)$ as $T \to 0$, the zero bias conductance must approach

$$\lim_{T \to 0} G(T) = 4G_0 \sin^2(\delta) = 4G_0 \sin^2\left(\frac{\pi}{4} N_{imp}\right) \quad (4)$$

which is indeed recovered in our calculations.

Results: We use a symmetric, constant lead density of states $\rho_0 = 1/(2D)$ with a band width $D = 30\Gamma_0$, $\Gamma_0 = 1meV \simeq 11.6K$ being the energy unit used throughout. We take $U = 10\Gamma_0 = 10meV$, corresponding to the experimental estimate of the charging energy $E_C \equiv U$ [12].

One of the striking, poorly understood features of the recent experiments on semiconducting carbon nanotube dots [12] is the thermal evolution of the zero bias conductance as a function of gate voltage. In the experiment, the orbitals are filled in groups of two (there being four such groups, I-IV [12]). In addition, the tunneling matrix elements increase with gate voltage. We restrict ourselves to a single representative group, keeping the tunneling matrix elements constant for simplicity; and calculate the zero-bias conductance as a function of the dimensionless gate voltage N_g, for different tunneling strengths $\Gamma = \Gamma_L + \Gamma_R$ and temperatures, using the NRG spectral functions: $G(T)/G_0 = -4 \int_{-\infty}^{\infty} d\omega \, (\partial f(\omega)/\partial\omega) \, t(\omega)$ with $t(\omega) = \pi \Gamma D(\omega)$ the t-matrix and $f(\omega)$ the Fermi function [24]. The results are given in Figs. 1 and 2 for three different coupling strengths $\Gamma = 0.5\Gamma_0, \Gamma_0, 2\Gamma_0$.

Our results concur well with experiment. Those for $\Gamma = 0.5meV$ (Fig. 1a) track the T-evolution of Group I depicted in Fig. 2 of Ref. [12]. Clear, pronounced Coulomb blockade peaks and valleys are seen in Fig. 1a. These disappear only at temperatures much lower than
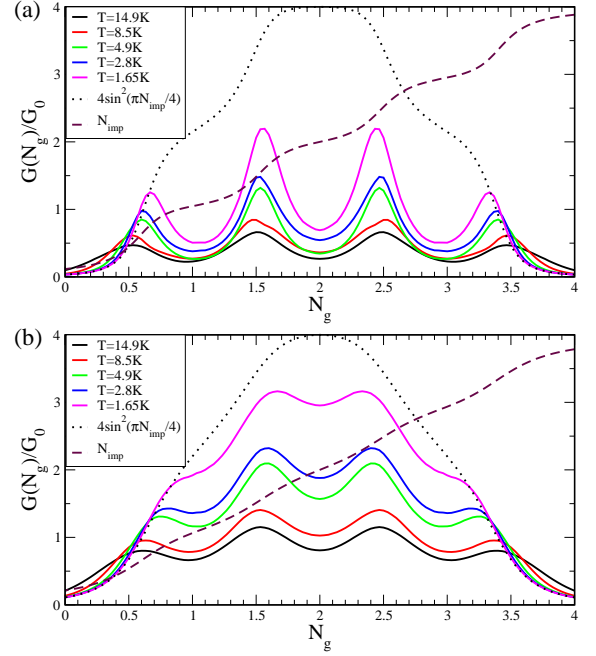

FIG. 1: (color online) Zero bias conductance *vs* dimensionless gate voltage N_g, for different T and two tunneling strengths $\Gamma = 0.5meV$ ((a)), $1meV$ ((b)); with $U \equiv E_C = 10meV$. The dotted line gives the $T = 0$ values, Eq. (4); N_{imp} is also shown (dashed line). NRG parameters [5, 21]: $\Lambda = 3$, $N_s = 2000$.

the experimental base $T = 1.3K$, indicative of strong correlations ($U/\Gamma = 20$ here) and hence small Kondo scales T_K in the middle of the valleys ($N_g = 1$ (3) and 2). The distance between the peaks is seen to become smaller with decreasing T, also in agreement with experiment. The origin is a pinning of the many-body Kondo resonance in $D(\omega)$ close to the chemical potential at low-T, evident in the t-matrix depicted in Fig. 5 (discussed below). For $T = 0$, the conductance from the Friedel sum rule Eq. (4) is shown as a dotted line in Fig. 1a. Absolute values of $G(T)$ also agree well with experiment. For Group I [12] the coupling asymmetry is $\Gamma_L/\Gamma_R \approx 2.5$, and hence $G_0 \simeq 0.8e^2/h$. With this, *eg* the calculated $N_g = 1.5$ (or 2.5) Coulomb blockade peak in $G(T)$ for $T = 1.65K$ translates to $G_{peak} \approx 1.7e^2/h$, in good agreement with experiment; and the widths of the peaks also concur with experiment. The slight experimental asymmetry of the $N_g = 0.5$ and 3.5 Group I conductance peaks can be attributed to a small increase in the tunnel coupling within the Group on increasing the gate voltage.

Results for $\Gamma = 1meV$ ($U/\Gamma = 10$, Fig. 1b) resemble the experimental Group III orbitals [12]. At higher T, remnants of the Coulomb blockade peaks remain visible; they are absent at base temperature. While for stronger correlations (*eg* Fig. 1a) the charge steps are quite pronounced, and the different orbital filling regimes well separated in the $T = 0$ conductance, for $U/\Gamma = 10$ orbital filling is almost continuous. The physical origin
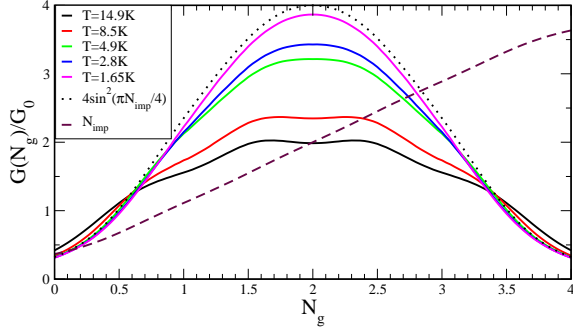
FIG. 2: (color online) Zero bias conductance vs N_g for different temperatures and $\Gamma = 2meV$. The dotted line gives the $T = 0$ values from Eq. (4). Other parameters as in Fig. 1.

of such behavior is in part the 'blocking effect' known from the theory of multi-channel models in the context of rare earth materials [13], in which Coulomb interactions lead to single-particle lifetime broadening of order $N\Gamma$, since N relaxation channels are present. In addition, the $SU(4)$ Kondo scale in the Kondo regime is much larger than for $SU(2)$ as the number of channels enters the exponent, $T_K^{SU(4)}/D \simeq [T_K^{SU(2)}/D]^{1/2}$ [4, 16]. In consequence, an $SU(4)$ model enters the weakly correlated regime for larger U/Γ than an $SU(2)$ symmetric model.

Fig. 2 shows results for a more weakly correlated $U/\Gamma = 5$. This tracks the T-evolution of the Group IV orbitals [12]. Here, consistent with experiment, charge fluctuations are significant and Coulomb blockade peaks in consequence absent, with the $G(T \to 0)$ limit Eqn. (4) being reached in practice at relatively high temperatures.

The T-dependence of $G(T)$ for the middle of the Coulomb valleys, $N_g = 2$ and $N_g = 1$ (or 3), is shown in Fig. 3a,b for 5 values of Γ. Comparison of the two shows the characteristic energy scales in all valleys are of the same order (see also Fig. 4 inset): the Coulomb blockade valleys are thus filled simultaneously with decreasing T, as seen in experiment [12]. This in turn provides strong evidence for $U' = U$, since only a very slight decrease of U' from the $SU(4)$ point $U' = U$ causes a sharp drop in the $N_g = 2$ Kondo scale towards $SU(2)$ form [16], while the $N_g = 1$ scale is by contrast barely affected [16, 19].

Defining a characteristic low-energy scale T_0 ($\propto T_K$) by $G(T_0)/G(0) = 0.5$, Fig. 3c shows the $N_g = 2$ results from Fig. 3a rescaled as $G(T)/G(0)$ vs $x = T/T_0$. On progressively decreasing Γ the data collapse, over an ever increasing T/T_0-interval, onto a common curve $g(x)$. This is the universal $SU(4)$ scaling conductance for $N_g = 2$. That limit is well reached, for all $T/T_0 < 10^2$ shown in Fig. 3c, by $\Gamma = 0.2meV$; but even for the largest Γ we consider ($2meV$, $U/\Gamma = 5$), the conductance scales onto the universal $g(x)$ over a significant x-range. Similar considerations arise for the $N_g = 1$ results, and the universal $SU(4)$ $g(x)$ for $N_g = 2$ and 1 (or 3) are shown in Fig. 4. For $x \gtrsim 1$, $g(x)$ for $N_g = 2$ and 1 asymptotically coincide, while for lower x the two are distinct (reflecting different
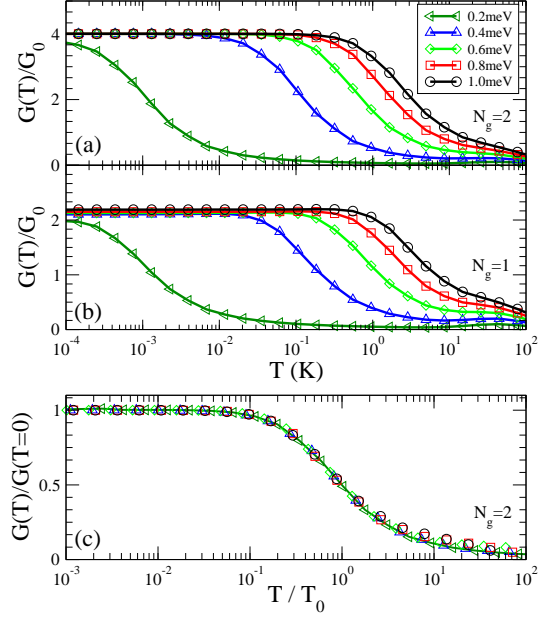

FIG. 3: (color online) T-dependence of $G(T)$ for five different values of Γ and two different dimensionless gate voltages: (a) $N_g = 2$ and (b) $N_g = 1$ (or $N_g = 3$). (c) Scaling the $N_g = 2$ results, $G(T)/G(0)$ vs $x = T/T_0$.
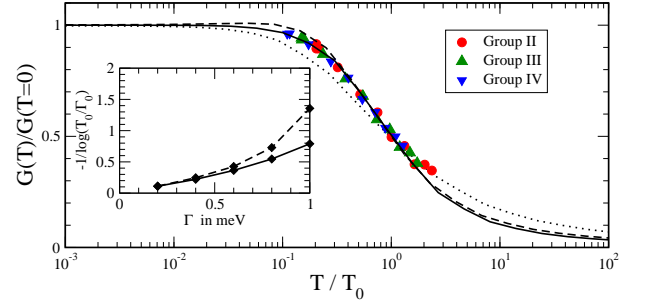

FIG. 4: (color online) $SU(4)$ scaling conductance $g(x) = G(T)/G(0)$ vs $x = T/T_0$ – solid line for $N_g = 2$, dashed for $N_g = 1$ (or 3). The $SU(2)$ scaling conductance is shown as a dotted line. Experimental results [12] for Groups II, III and IV (with $N_g = 2$) are also shown. Inset: evolution of the low-energy scale T_0, for $N_g = 2$ (solid) and $N_g = 1$ (dashed).

leading corrections to the $SU(4)$ fixed point). The corresponding universal $g(x)$ for a symmetric $SU(2)$ model is also shown. It is seen to have a quite different form, and is known [12] not to fit well the carbon nanotube data. For the $SU(4)$ model by contrast, our results agree well with experiment – as seen in Fig. 4 where data for Groups II, III and IV in the middle of the two-electron valleys [12] are compared to the $N_g = 2$ $SU(4)$ $g(x)$. At sufficiently high T, departure from universal scaling must inevitably occur (as above, and just visible for the Group II, III data), but the data collapse remarkably well onto the scaling conductance [29].

Finally, to assess approximately the effects of a finite source-drain bias $V_{sd} \equiv V$, we neglect explicit depen-
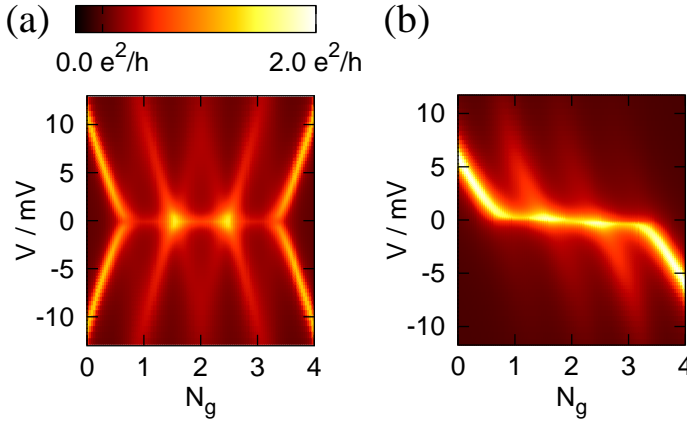
(a)

0.0 e^2/h   2.0 e^2/h

(b)

FIG. 5: (color online) Color-coded contour plot in the (V, N_g)-plane of (a) $t_s(V, N_g)$ for $\Gamma = 0.5meV$ at $T = 2.8K$, as in Fig. 1a; (b) $t(\omega = eV)$ for $\Gamma = 1meV$ as in Fig. 1b.

dence of the self-energy on V. Granted this, if one of the contacts is sufficiently open that it acts as a tunneling probe, the $T = 0$ conductance $G(V, N_g) \propto t(\omega = eV)$ with $t(\omega)$ the t-matrix as above. This situation is appropriate to the Group III and IV orbitals of [12]. If by contrast the contacts are more symmetrically coupled, then $G(V, N_g) \propto t_s(V, N_g) = \frac{1}{2}[t(\omega = +\frac{1}{2}eV) + t(\omega = -\frac{1}{2}eV)]$ [24]. This we believe is the relevant case for the Group I orbitals of [12]. For $\Gamma = 0.5meV$ (as in Fig. 1a), Fig. 5a shows a contour plot of $G_0 t_s(V, N_g)$ (calculated for $T = 2.8K$ [30]). The striking similarity to the experimental Group I differential conductance map (Fig.2b of [12]) is evident, including the clear Coulomb blockade diamonds. For $\Gamma = 1meV$ (as in Fig. 1b), Fig. 5b shows a corresponding contour plot of $G_0 t(\omega = eV)$; this in turn captures well the Group III conductance map [12].

Conclusion: Motivated by recent experiments on carbon nanotube quantum dots [12], we have studied the evolution of an $SU(4)$ Anderson model from correlated Kondo to mixed valent behavior, on progressive increase of the dot-lead tunnel couplings. NRG results obtained are in compelling agreement with experiment [12], from the thermal evolution and scaling behavior of the zero-bias conductance, to differential conductance maps; and show that an $SU(4)$ Anderson model provides a remarkably faithful description of carbon nanotube dots.

[1] C. Dekker, Phys. Today **52**, 22 (1999).
[2] S. J. Tans et al., Nature **386**, 474 (1997).
[3] M. A. Kastner, Rev. Mod. Phys. **64**, 849 (1992).
[4] A. C. Hewson, *The Kondo Problem to Heavy Fermions* (Cambridge Press, Cambridge UK, 1993).
[5] K. G. Wilson, Rev. Mod. Phys. **47**, 773 (1975).
[6] J. Nygard, D. Cobden, and P. Lindelhof, Nature **408**, 342 (2000).
[7] L. P. Kouwenhoven and L. I. Glazman, Phys. World **14**, 33 (2001).
[8] W. J. Liang, M. Bockrath, and H. Park, Phys. Rev. Lett. **88**, 126801 (2002).
[9] M. R. Buitelaar et al., Phys. Rev. Lett. **88**, 156801 (2002).
[10] P. Jarillo-Herrero et al., Nature **434**, 484 (2005).
[11] A. Makarovski, A. Zhukov, J. Liu, and G. Finkelstein, Phys. Rev. B **75**, 241407 (2007).
[12] A. Makarovski, J. Liu, and G. Finkelstein, Phys. Rev. Lett. **99**, 066801 (2007).
[13] N. E. Bickers, Rev. Mod. Phys. **59**, 845 (1987).
[14] D. Boese, W. Hofstetter, and H. Schoeller, Phys. Rev. B **66**, 125315 (2002).
[15] L. Borda et al., Phys. Rev. Lett. **90**, 026602 (2003).
[16] M. R. Galpin, D. E. Logan, and H. R. Krishnamurthy, Phys. Rev. Lett. **94**, 186406 (2005).
[17] R. Lopez et al., Phys. Rev. B **71**, 115312 (2005).
[18] M. S. Choi, R. Lopez, and R. Aguado, Phys. Rev. Lett. **95**, 067204 (2005).
[19] A. K. Mitchell, M. R. Galpin, and D. E. Logan, Europhys. Lett. **76**, 95 (2006).
[20] C. A. Büsser and G. B. Martins, Phys. Rev. B **75**, 045406 (2007).
[21] R. Bulla, T. Costi, and T. Pruschke, cond-mat/0701105 (2007).
[22] Y. Oreg, K. Byczuk, and B. I. Halperin, Phys. Rev. Lett. **85**, 365 (2000).
[23] A. Makarovski, L. An, J. Liu, and G. Finkelstein, Phys. Rev. B **74**, 155431 (2006).
[24] Y. Meir and N. S. Wingreen, Phys. Rev. Lett. **68**, 2512 (1992).
[25] R. Peters, T. Pruschke, and F. B. Anders, Phys. Rev. B **74**, 245114 (2006), A. Weichselbaum and J. von Delft, Phys. Rev. Lett. **99**, 076402 (2007).
[26] F. B. Anders and A. Schiller, Phys. Rev. Lett. **95**, 196801 (2005), Phys. Rev. B **74**, 245113 (2006).
[27] D. C. Langreth, Phys. Rev. **150**, 516 (1966).
[28] F. B. Anders, N. Grewe, and A. Lorek, Z. Phys. B Condensed Matter **83**, 7 (1991).
[29] Results for Group I (smallest Γ) lie slightly outside the scaling regime for most of the experimental T-range.
[30] Additional thermal smearing of $G(V, N_g)$ from finite-T Fermi functions is a minor effect.